JOURNAL OF MATERIALS SCIENCE 24 (1989) 671–680

Contribution of damage by multiple crack growth to the strain-rate sensitivity of a polycrystalline alumina at elevated temperatures

D. P. H. HASSELMAN, A. VENKATESWARAN, K. Y. DONALDSON
Department of Materials Engineering, Virginia Polytechnic Institute and State University, Blacksburg, Virginia 24061, USA

The strength of a polycrystalline aluminium oxide measured in four-point bending at elevated temperatures over a range of displacement-controlled loading rates was observed to exhibit an unusually high strain-rate dependence. Scanning electron microscopy revealed that at the lower values of strain-rate, failure was accompanied by the formation of a number of additional macrocracks adjacent to the plane of fracture. Separate measurements of specimens deformed to approximately 75% of the fracture strain indicated that, at these lower values of strain rate, the effective Young's modulus was decreased by as much as a factor of two. It is suggested that the high strain-rate sensitivity was the direct result of a strain-rate dependent decrease in Young's modulus and associated effect of "strain-softening" for conditions of displacement-rate controlled mechanical loading. The validity of this hypothesis was verified by a fracture-mechanics analysis of a mechanical model subjected to displacement-controlled tensile loading, with elastic behaviour expressed in terms of the effect of cracks on continuum elastic properties.

1. Introduction

Brittle materials at stress levels below the instantaneous fracture stress exhibit slow crack extension, referred to as "sub-critical crack growth", with a rate strongly dependent on environmental conditions such as humidity and temperature [1]. Under conditions of dynamic loading, such as constant stress or strain-rate testing, sub-critical crack growth leads to a loading-rate dependence of the failure stress, generally referred to as "strain-rate sensitivity" [2–5].

In principle, the "strain-rate sensitivity" of a given material can be derived on the basis of well-known principles of fracture mechanics, provided that information exists on the crack-growth behaviour, the critical stress intensity factor and the crack-size geometry and/or instantaneous fracture stress [6, 7]. In doing so, however, a careful distinction must be made between loading conditions of constant stress rate and constant strain rate. The presence of a crack, depending on its size relative to the specimen size, can have a significant effect on the compliance of the specimen. For constant stress-rate loading conditions, any change in specimen compliance due to crack growth is corrected for automatically by the appropriate instrumentation, such as that found in servo-electric-hydraulic mechanical testers, so that the sample loading rate is not affected by a change in specimen compliance. However, under conditions of constant strain rate, usually achieved with the aid of displacement-controlled mechanical testers, at any given value of displacement an increase in specimen compliance will cause a corresponding decrease in the applied load and loading rate.

The role of specimen compliance in crack-propagation behaviour is well recognized in the general field of fracture mechanics and in evaluation of crack-propagation behaviour and fracture toughness [8–10]. Furthermore, Evans [7] analysed the effect the increase in specimen compliance due to the sub-critical growth of a single failure-initiating flaw has on strain-rate sensitivity. The results of this analysis showed that for crack sizes at failure, l_f, less than 10% of the specimen thickness, W, the increase in specimen compliance is sufficiently small that the stress rate and strain rate are simply related by Young's modulus of the material of the test specimen such that the stress-rate sensitivity of the failure stress can be obtained with the use of displacement (stress)-controlled mechanical testers and vice-versa. For $l_f > 0.1\ W$, however, the stress rate and strain rate can no longer be related simply by Young's modulus, and the effect of increased compliance must be taken into account when using constant displacement rate tests to obtain strain-rate sensitivity data.

Rather than failing from the formation and growth of a single crack, many brittle materials can undergo simultaneous growth of a number of cracks. Such multiple cracks can arise from a number of sources,

0022–2461/89 $03.00 + .12

such as surface damage [11] or processing flaws [12]. High densities of microcracks can form, either spontaneously or under the influence of an applied stress, as the result of internal stresses due to a spatially non-uniform thermal expansion in polycrystalline single-phase materials [13] or brittle matrix composites [14]. Cracks can also be initiated at stress concentrations in heterogeneous materials such as concrete [15] and rock [16]. At elevated temperatures, microcrack formation can result from grain-boundary sliding [17], stress-induced growth of residual pores or by cavitation [18]. Coalescence of such microcracks can result in the formation of macrocracks.

The presence of cracks, as demonstrated analytically and experimentally, can cause a significant lowering of the effective elastic moduli of materials [19–23]. For this reason, multiple crack formation and/or growth should lead to an increase in the compliance of the mechanical test specimens of brittle materials. This effect, in brittle materials which do not deform plastically, such as concrete and rock, when subjected to mechanical loading at a constant displacement rate, leads to a type of non-linear stress–strain behaviour referred to as "strain softening", i.e. a decrease in the value of the load at any given value of displacement compared to the value expected from Young's modulus of the untested crack-free materials [15, 16, 24, 25].

In a recent study [26], which focused on the fractography of the role of cracks in the non-linear deformation of polycrystalline ceramics, we found that the fracture stress exhibited what appeared to be a rather high strain-rate sensitivity. Furthermore, it was noted that deformation was also accompanied by a strain-rate dependent formation of multiple macrocracks along the length of the specimen, in addition to the formation of the failure-causing crack. It was speculated that the formation of these macrocracks and associated increase in specimen compliance could explain, at least in part, the observed high strain-rate sensitivity.

The purpose of this investigation was to conduct an experimental study of this effect and to present an analysis for conditions of uniaxial tensile loading.

2. Experimental details

2.1. Material

The test material chosen for this study consisted of a substrate-quality, relatively fine-grained polycrystalline aluminium oxide known as AlSiMag 838 (General Electric Corp., Chattanooga, Tennessee, USA). The scanning electron micrograph of a room-temperature fracture surface shown in Fig. 1 indicates that this material is nearly fully dense with an average size of $\sim 5\,\mu m$ and an occasional grain as large as $20\,\mu m$. For purposes of future comparison, Fig. 2 shows a scanning electron micrograph of a polished section through an annealed undeformed specimen, which indicates the presence of an occasional pore without any preferred pore orientation.

The test samples were circular rods with a length of ~ 50 mm and a diameter of ~ 4.8 mm. Prior to testing, all samples were annealed at about 1000° C for 6 to 7 h to minimize the effect of residual stresses, if any.

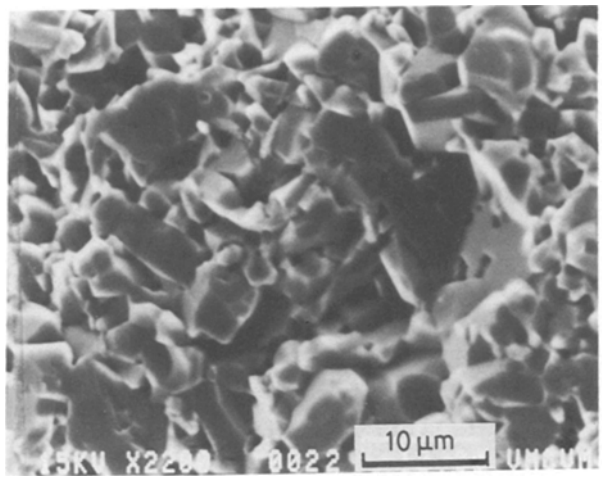

Figure 1 Room temperature scanning electron fractograph of 838 alumina.

2.2. Test procedures

The specimens were tested in four-point bending with inner and outer spans of 10 and 40 mm, respectively. The specimen holder consisted of graphite, the load to the specimens being transferred by graphite pins which were permitted to rotate freely in order to keep extraneous stresses to a minimum. Testing was done in an argon atmosphere within an environmental chamber resistively heated with tungsten-mesh heating elements. The environmental chamber was contained within the load-frame of an electro-hydraulic closed-loop mechanical tester made by the MTS Corporation. The displacement of the actuator and the resulting load were transferred via graphite push-rods and water-cooled bellows to the specimen and load cell, respectively. The displacement of the actuator was measured using a displacement gauge, held against the actuator outside the environmental chamber. This gauge, with a range of ~ 4 mm, permitted measurement of the displacement to within a few micrometres. By making a separate measurement of the elastic displacement of the total load train without the specimen, the displacement of the loading points of the specimens could be obtained by the

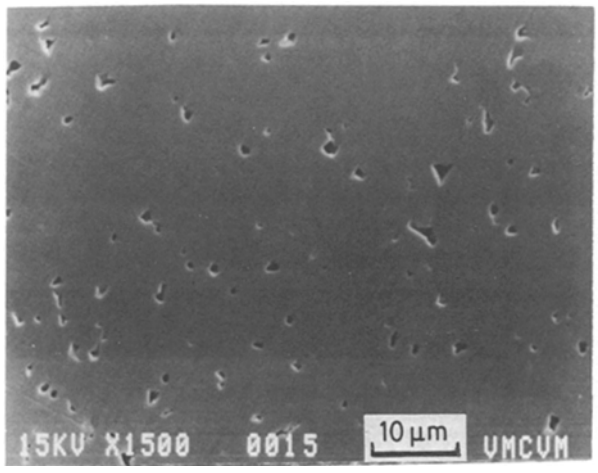

Figure 2 Scanning electron micrograph of a polished section through as-received 838 alumina.

appropriate subtraction. For the test material and specimen size of this study, the elastic displacement of the specimen and load train were approximately equal in value. The load as a function of displacement was recorded with an x–y recorder for most values of displacement rate and with an oscilloscope at the highest values of displacement rate. For purposes of measuring the strain-rate sensitivity, the specimens were loaded over a range of values of constant displacement rates at temperatures of 1350, 1400 and 1450° C. The displacement–load data were converted to strain and stress using the theory for pure bending of homogeneous beams.

In order to determine possible changes in the effective Young's modulus during deformation, specimens were deformed at 25, 1400 and 1450° C over the lower range of strain rates (0.0016 to 0.08 min^{-1}) to approximately 75 to 85% of the failure strain observed in the fracture studies. The effective Young's modulus at room temperature of these deformed samples was then obtained from load–displacement data obtained from four-point bending tests identical to the deformation at high temperatures. Changes in Young's modulus for strain rates in excess of 0.08 min^{-1} could not be obtained due to experimental difficulties encountered in deforming the specimens to prescribed small values of displacement. Possibly because of scattering at the cracks which formed during high-temperature deformation, Young's modulus could not be measured by acoustic techniques.

Following testing, the specimen external and fracture surfaces (if broken) were examined by scanning electron microscopy. The specimens were also sectioned by a slow-speed diamond saw and then diamond-polished to provide a cross-section of the specimen interior ranging from the line of maximum tensile stress to the line of maximum compressive stress.

3. Results and discussion

3.1. Deformation, fracture stress and fractography

Figs 3a, b and c show typical stress–strain behaviour for a range of values of strain rate at 1350, 1400 and 1450° C, respectively. Considerable non-linearity can be noted. Fracture resulted for all but the lowest values of strain rate, at which the stress developed did not exceed the failure stress over the duration of the experiment. It should also be noted that a number of stress–strain curves just prior to fracture showed a decrease in stress with increasing strain. This latter

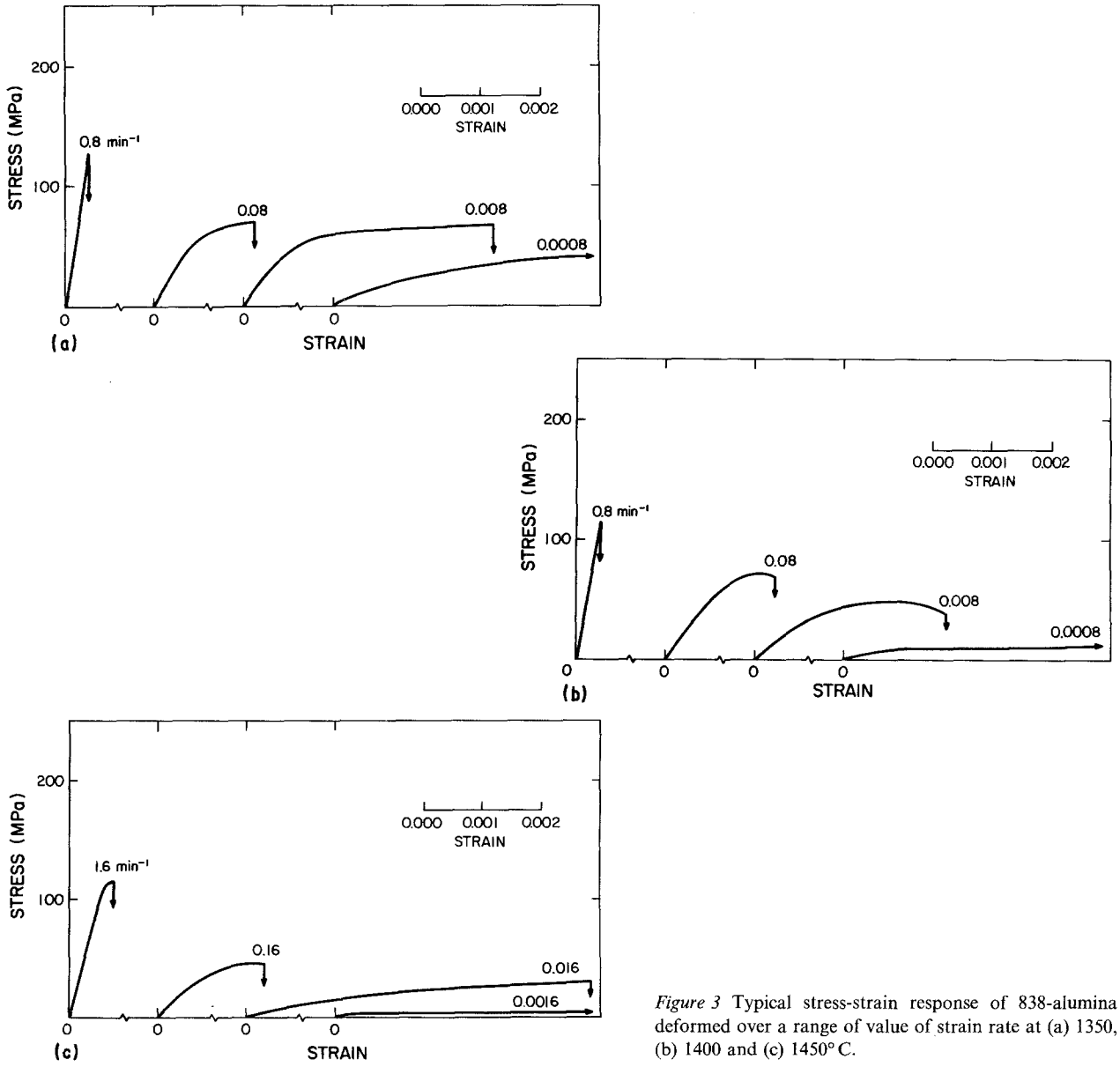

Figure 3 Typical stress-strain response of 838-alumina deformed over a range of value of strain rate at (a) 1350, (b) 1400 and (c) 1450° C.

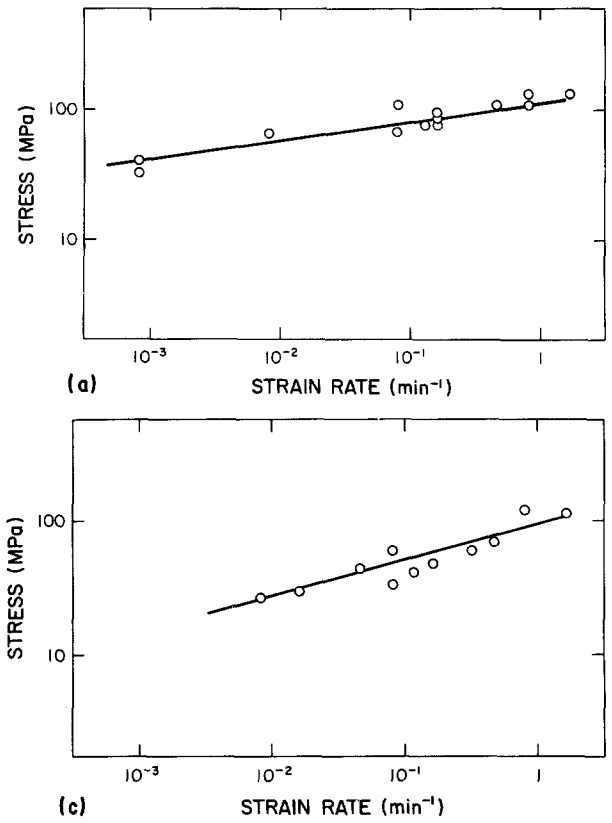

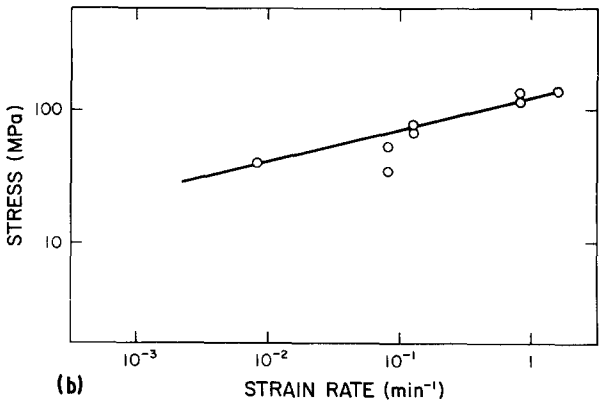

Figure 4 Dependence of fracture stress of 838-alumina on strain rate at (a) 1350, (b) 1400 and (c) 1450° C.

effect is not expected for generally accepted mechanisms of creep, but in the absence of major changes in specimen geometry, as is the case in this study, can result only from an increase in specimen compliance, due to be discussed subsequently.

Figs 4a, b and c show the magnitude of the failure stress for the specimens which exhibited fracture as a function of strain rate, calculated from the displacement rate, and plotted on a log–log basis for 1350, 1400 and 1450° C, respectively.

Experimental data for the failure stress as a function of loading rate can be used to evaluate the magnitude of the stress-intensity exponent, N, in the dependence of the rate of sub-critical crack growth, V, on the stress-intensity factor, K_I [6]. Initially the assumption will be made that the cracks do not significantly affect the specimen compliance, such that the strain rate, $\dot{\varepsilon}$, is given by

$$\dot{\varepsilon} = \dot{\sigma}/E_0 \quad (1)$$

The relationship of sub-critical crack velocity, V, and mode I stress-intensity factor, K_I, was assumed to be

$$dl/dt = AK_I^N \quad (2)$$

where N is the stress-intensity factor exponent.

The dependence of the fracture stress, σ_f, on strain rate (for certain simplifying assumptions discussed in the original studies [6]) can be derived to be

$$\sigma_f^{N+1} = CE_0\dot{\varepsilon} \quad (3)$$

where C is a constant for a given material and environment.

Equation 3 indicates that the slope of the plot of log (σ_f) against log ($\dot{\varepsilon}$) equals $1/(N + 1)$. This relationship, for the slopes of the data in Figs 4a, b and c, yields values of N equal to 5, 2.7 and 2.3 for 1350, 1400 and 1450° C, respectively. These values are generally far lower than those obtained for alumina and other brittle materials at ambient or elevated temperatures [4, 7, 27–31].

Scanning electron microscopy of the surfaces of the fractured specimens revealed that deformation was accompanied by a strain-rate dependent formation of cracks adjacent to the plane of fracture.

Figs 5a and b show polished sections of specimens deformed at 1350° C at strain rates of 0.08 and 0.8 min^{-1}, respectively, with the right-hand side of the figure at or near the line of maximum tensile stress.

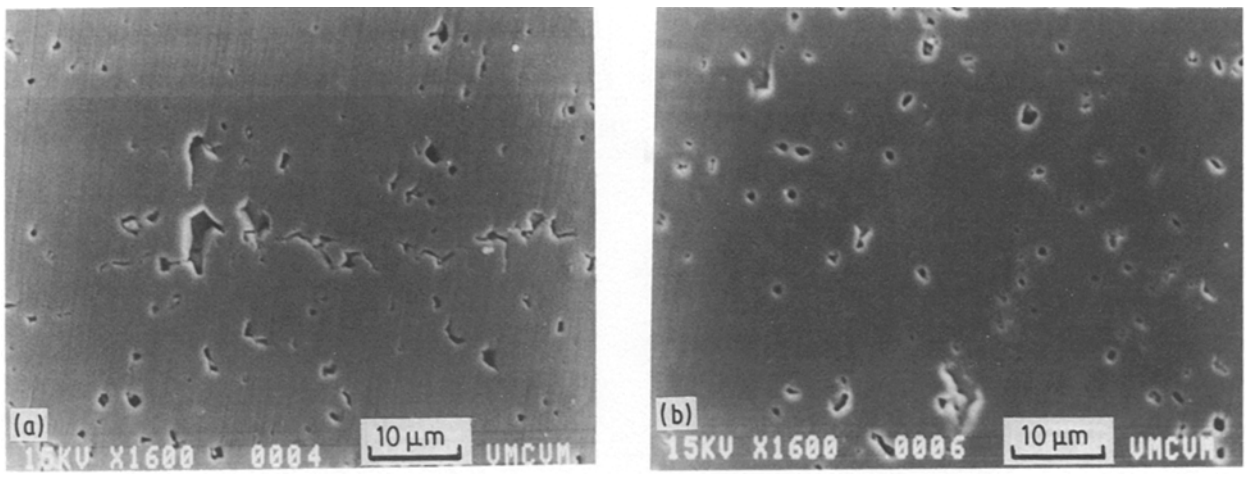

Figure 5 Scanning electron micrographs of polished sections through the line of maximum tensile stress at the micrograph's right-hand edge of specimens deformed at 1350° C and (a) 0.08 and (b) 0.8 min^{-1}.

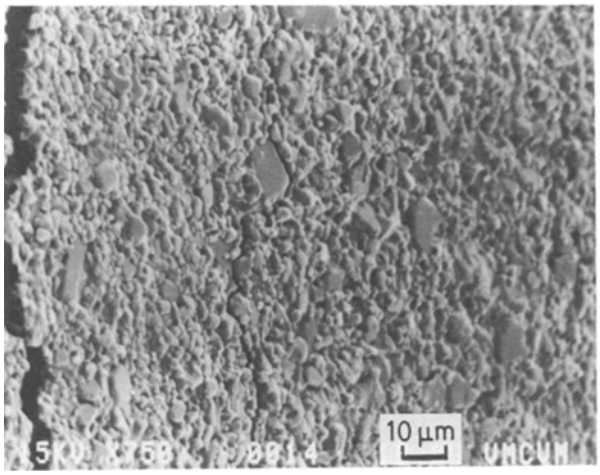

Figure 6 Scanning electron micrograph of the tensile surface of a specimen deformed at 1350° C and 0.08 min^{-1}.

The specimen deformed at the lower value of strain rate shows some evidence for intergranular cracking perpendicular to the tensile stress, whereas such crack formation is absent in the specimens deformed at 0.8 min^{-1}.

Fig. 6 shows a scanning electron micrograph of the tensile specimen surface adjacent to the plane of fracture of the same specimen shown in Fig. 5a. The specimen surface gives evidence for development of at least two additional cracks in addition to the plane of fracture. One such crack appears to have been nucleated at a large grain.

As indicated by their dimensions relative to the scale of the microstructure as well as their preferred path of propagation, crack formation in the alumina tested under the conditions of this study appears to occur by the growth of macrocracks along the grain boundaries rather than by the formation of isolated intergranular cracks of the order of the grain size, such as those observed by Folweiler and others [31, 32]. No crack formation could be detected in the regions of the specimens of Figs 5a and 6 subjected to compressive loading.

Figs 7a and b show polished sections of a specimen deformed at ~1400° C at strain rates of 0.08 and 0.8 min^{-1}, respectively. Again, crack formation was found only at the lower strain rate, and was absent at the higher value. A surface crack in the specimen deformed at 0.08 min^{-1} is shown in Fig. 8.

At 1450° C crack formation was extensive, as indicated by scanning electron micrographs of sections of the specimen interiors and surfaces shown in Figs 9 and 10, respectively. Crack formation occurred at strain rates of 0.08, 0.16 and 0.32 min^{-1}, but was absent at 1.6 min^{-1}. For all three temperatures the number of cracks formed along the central portion of the bend-specimen ranged from two to four.

In general, the microstructural evidence suggests that multiple crack formation in those specimens which exhibited fracture occurred at the lower values of strain rate, but was absent (or could not be detected) at the higher values of strain rate. Furthermore, crack formation appeared to be more pronounced at 1400 and 1450° C than at 1350° C. In terms of a possible interpretation of these results, it should be noted that no crack formation could be detected in those specimens deformed at the lowest strain rates, which did not exhibit fracture over the time period of the deformation and for which no strength data could be obtained. It is postulated that for these specimens, the strain rate was sufficiently low that deformation could occur by diffusional creep at stress levels below those required for crack nucleation. It appears, then, that crack formation occurred only over the intermediate values of strain rate of this study, at which the stress exceeded the minimum values required for multiple crack nucleation and for which the time to failure was sufficiently long for significant crack propagation to occur.

Fig. 11 shows the data for the effective Young's modulus of specimens deformed at 25, 1400 and 1450° C, over a range of strain rates up to 0.08 min^{-1}, to approximately 75 and 85% of the fracture strain established during the measurements of the strain-rate sensitivity. The data obtained at 25° C show an average value, independent of strain rate, of ~400 GPa which compares very favourably with general literature values for Young's modulus of fully dense polycrystalline aluminium oxide. The absence of an effect of strain rate on Young's modulus is reflective of the absence of any microstructural changes during deformation at 25° C.

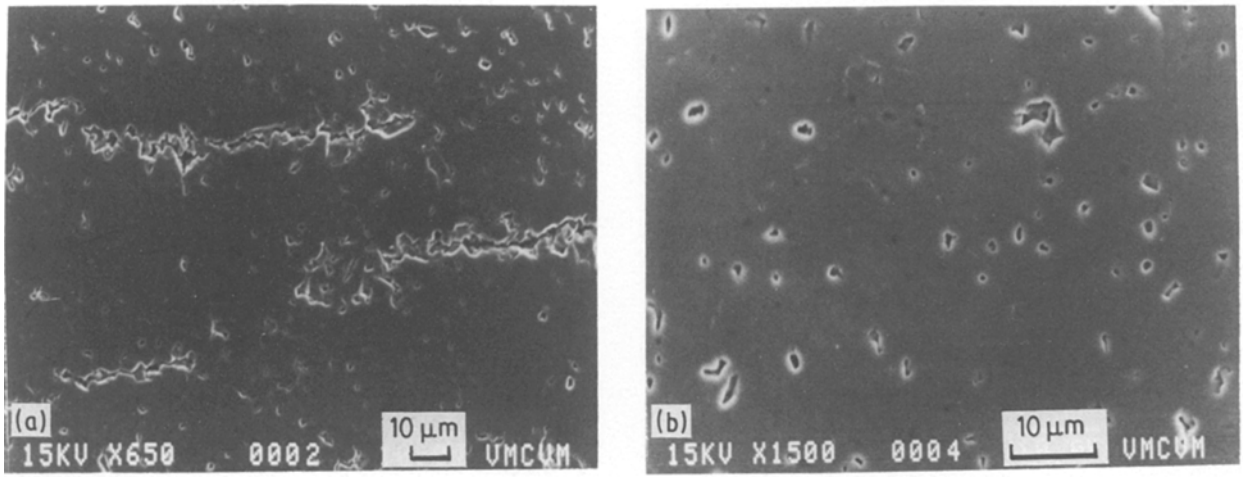

Figure 7 Scanning electron micrographs of polished sections through the line of maximum tensile stress at the micrograph's right-hand edge of specimens deformed at 1400° C, and (a) 0.08 and (b) 0.8 min^{-1}.

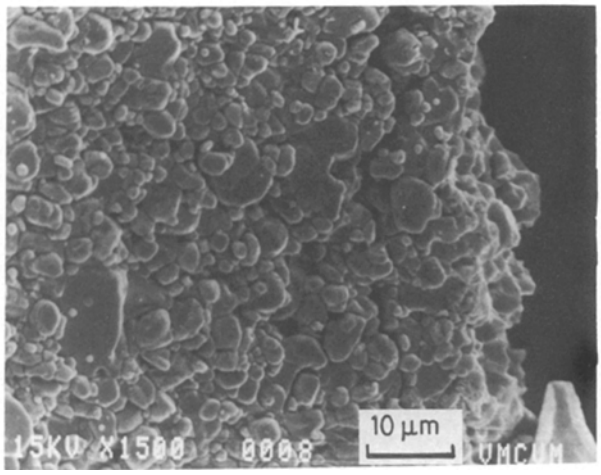

Figure 8 Scanning electron micrograph of tensile surface near the fracture plane of a specimen deformed at 1400° C and 0.08 min^{-1}.

At 1400 and 1450° C, however, a pronounced loading-rate effect is present. This is especially so for the data at 1450° C where Young's modulus is decreased from the value for the crack-free material by as much as a factor of two at the lowest value of strain rate. This must have a significant effect on the magnitude of stress reached under the conditions of displacement-controlled loading of this study. For 1400° C, Young's modulus of the specimen deformed to ~85% of the failure strain is some 10% below the value for the specimens deformed at ~75% of the failure strain. This effect does not appear to be present for the data of the specimens deformed at 1450° C.

Extrapolation of the data for Young's modulus following deformation at 1400 and 1450° C to higher values of strain rate suggests that a strain rate of ~0.2 min^{-1} would result in a value of Young's modulus ~400 GPa, as found for the crack-free material. This implies that no significant multiple crack formation would occur at strain rates > 0.2 min^{-1}, which confirms the fractographic evidence presented earlier that no crack formation occurred at the higher values of strain rate of this study.

It should be pointed out that the data shown in Fig. 11 represent the effective Young's modulus at strains of ~75% and ~85% of the fracture strain. It is speculated that if data could have been obtained for specimens deformed to within a few per cent of the failure strain, they may well have been significantly lower.

In view of the above observations, at least two explanations can be given for the high strain-rate sensitivity, i.e. low values of N for the failure stress as observed in this study. Firstly, prior to fracture, the specimen can deform by creep. Under conditions of loading by a constant strain rate, if the fracture and creep processes are independent, creep deformation will result in a lower stress value than would have been obtained in the absence of creep. Because the total amount of creep deformation at any given temperature prior to fracture will decrease with increasing displacement rate, an enhancement of the dependence of fracture stress on strain rate is expected, thereby resulting in a decrease in the apparent value of N.

The second explanation for low values of N is based on the effect sub-critical growth of multiple cracks has on the compliance of the specimen prior to fracture. Here, as for creep deformation, the relative amount of the sub-critical growth of multiple cracks and resulting increase in specimen compliance as manifested by the decrease in effective Young's modulus and associated decrease in stress will increase with decreasing strain rate. In turn, this will decrease the apparent value of the stress intensity exponent, N, obtained from the experimental data for the strain-rate sensitivity. The results for the fractography and the observed strain-rate dependent decrease in Young's modulus provide supporting evidence for the latter hypothesis.

Consequently, the observed strain-rate sensitivity is expected to be governed by the combined effects of diffusional creep and strain-rate dependent "strain softening". An estimate of the relative contribution of both these effects may be difficult to evaluate. Nevertheless, an estimate can be obtained of the stress–strain response in the absence of crack formation assuming deformation occurs by the dominant mechanism of diffusional creep, which for the mean grain size and temperature of the alumina of this study occurs by Coble creep controlled by diffusion of the

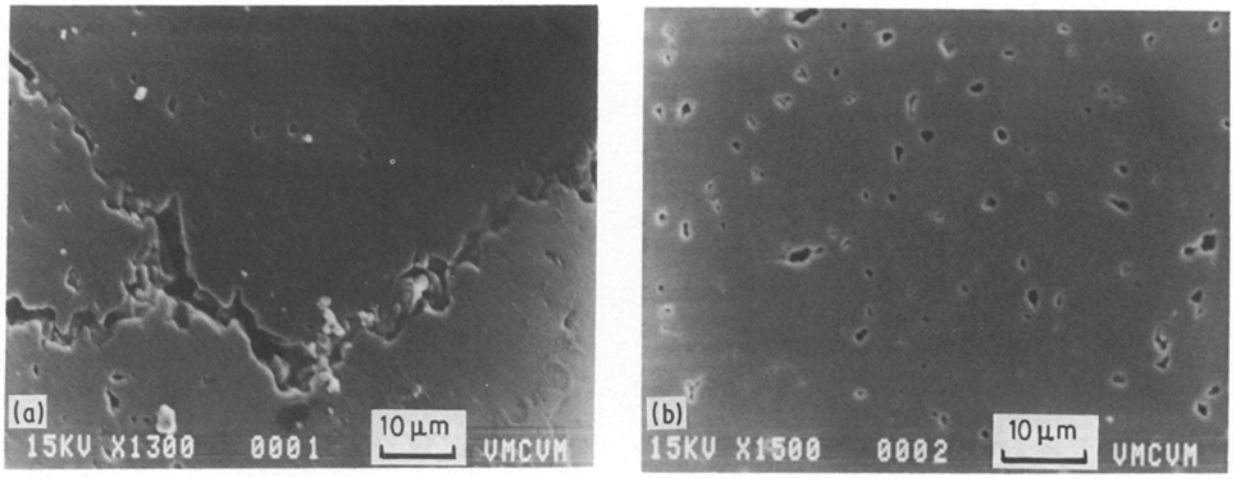

Figure 9 Scanning electron micrographs of polished sections through the line of maximum tensile stress at the micrograph's right-hand edge of specimens deformed at 1450° C and (a) 0.08 and (b) 1.6 min^{-1}.

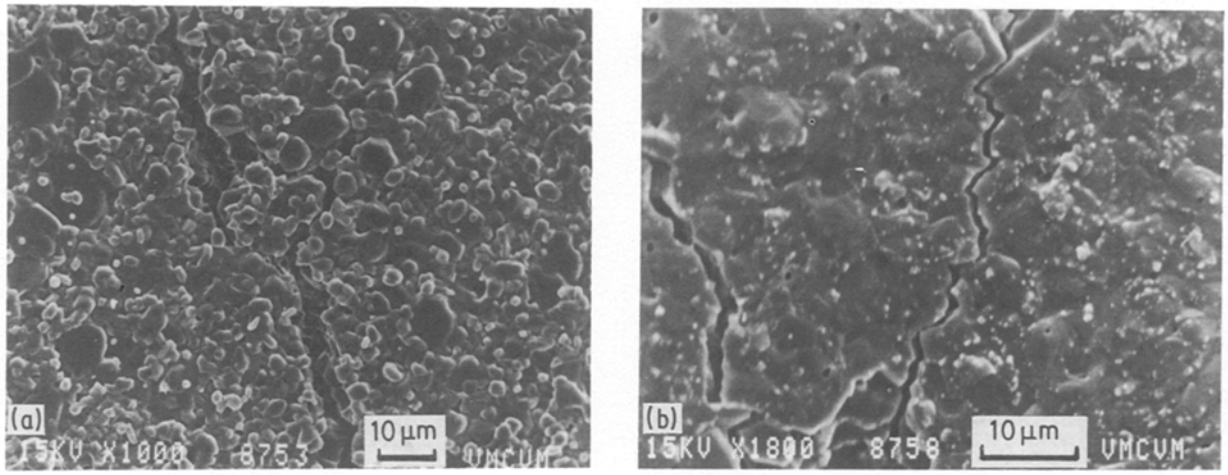

Figure 10 Scanning electron micrographs of the tensile surface of specimens deformed at 1450° C and (a) 0.16 and (b) 0.32 min^{-1}.

Al^{3+} ion [33]. The creep rate ($\dot{\varepsilon}_c$) at any given value of stress (σ) is expressed by

$$\dot{\varepsilon}_c = 24\sigma\Omega D_{gb}/d^3kT \quad (4)$$

where the symbols and numerical values taken from the study of Langdon and Mohamed [34] are: σ is the applied stress, Ω is the molecular volume = 4.2×10^{-29} m^3, d is the grain size = 5 μm, k = the Boltzmann constant = 1.38×10^{-23} J $atom^{-1}$ °K^{-1}, T = absolute temperature (1673°K used for calculations), D_{gb} is the grain-boundary diffusivity for the Al^{3+} ion = $8.6 \times 10^{-10} \exp(-419\,000/8.314T)$.

For constant strain rate, $\dot{\varepsilon}$, the dependence of stress on time, t, can be derived to be

$$\sigma(t) = \eta\varepsilon_c[1 - \exp(-E_0 t/\eta)] \quad (5)$$

where η is the effective viscosity with $\eta = \sigma/\dot{\varepsilon}$.

The stress response for a material subjected to a constant strain rate and associated creep response given by Equation 4 was calculated for the range of strain rates and specimen configuration of this study.

Fig. 12 shows the results obtained. Comparison with the stress–strain results presented in Fig. 3 shows that in the absence of cracks the stress reached far exceeds the values observed in this study. Even if Equation 4 were in error by as much as an order of magnitude, it can be concluded that diffusional creep made only a minor contribution to the stress–strain behaviour at the intermediate values of strain rate, leaving the effect of strain softening due to crack formation as the primary mechanism.

3.2. Analysis

The mechanical model selected for this analysis consisted of a linearly elastic solid containing non-interacting penny-shaped cracks of equal size, oriented perpendicular to a uniaxially applied tensile stress. In analogy to earlier studies of the effect of cracks on continuum elastic properites, Young's modulus (E) of the cracked solid was assumed to be described by

$$E = E_0(1 + \alpha)^{-1} \quad (6)$$

where E_0 is Young's modulus of the crack-free material. For parallel penny-shaped cracks oriented perpendicular to the applied stress, the quantity, α [22] is given by

$$\alpha = 16(1 - \nu_0^2)N_c l^3/3 \quad (7)$$

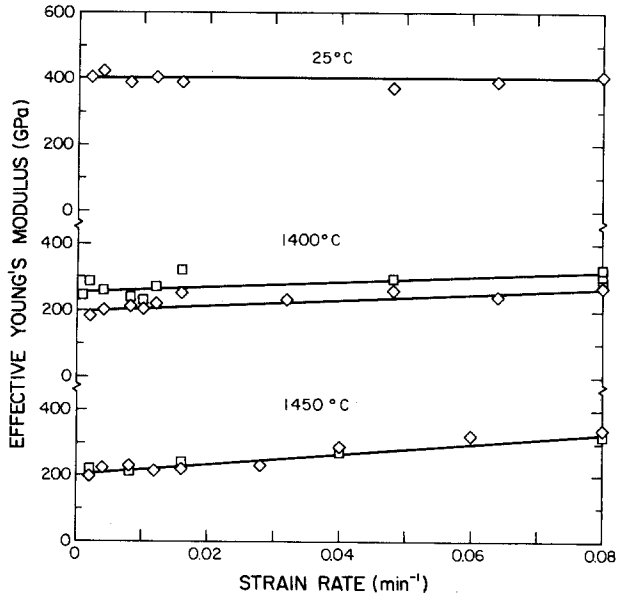

Figure 11 Effective Young's modulus at room temperature following deformation over a range of strain rates to approximately (□) 75 and (◇) 85% of the failure strain at 25, 1400 and 1450° C.

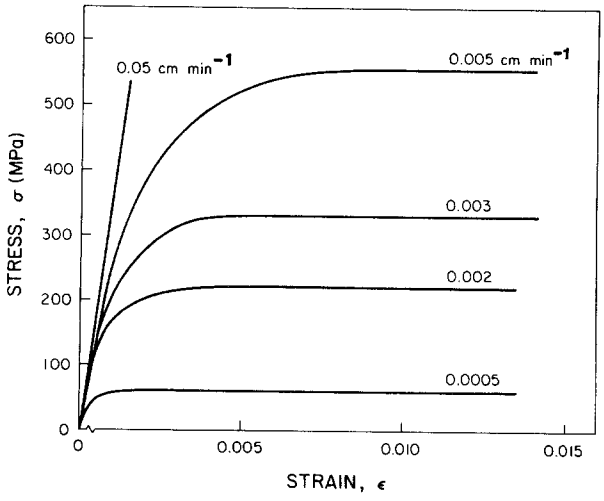

Figure 12 Calculated stress–strain response for non-linear deformation controlled by Coble creep.

TABLE I Typical values for polycrystalline alumina used for calculation of strain-rate sensitivity at 1400° C.

Critical stress intensity factor, K_{IC}	2×10^6 N m$^{-3/2}$
Stress intensity exponent, N	10
Constant A in $V = AK_I^N$	10^{-67} MKS units
Young's modulus, E_0	330 GPa
Crack radius, l_0	50 μm
Geometric constant, Y	1.09
Poisson's ratio	0.26

where v_0 is Poisson's ratio of the crack-free material, N_c is the number of cracks per unit volume and l is the radius of the cracks, where $l = 1(t)$ and t is the time. At $t = 0$, the initial value for α is taken as α_0.

The model was assumed to be initially stress-free and subjected to deformation under a constant strain rate, $\dot{\varepsilon}$, at $t = 0$.

The stress, $\sigma(t)$, becomes

$$\sigma(t) = \dot{\varepsilon} t E_0 (1 + \alpha)^{-1} \quad (8)$$

The stress-intensity factor, K_I, stress, $\sigma(t)$, and crack size, l, are related by

$$K_I = Y\sigma l^{1/2} \quad (9)$$

where Y is a geometric constant, which from the solution of Sack for a penny-shaped crack [35] can be derived to be equal to $2(1 - v_0^2)^{1/2}/\pi^{1/2}$.

Substitution of Equations 8 and 9 into Equation 2 yields

$$dl/dt = AY^N \dot{\varepsilon}^N t^N E_0^N l^{N/2} (1 + \alpha)^{-N} \quad (10)$$

which reduces to

$$\int_{l_0}^{l} (1 + \alpha)^N l^{-N/2} dl = AY^N \dot{\varepsilon}^N E_0^N t^{N+1}/(N + 1) \quad (11)$$

A solution for the integral in Equation 11 can be obtained from the tables compiled by Groebner and Hofreiter [36]. This solution, too complex for reproduction here, was programmed for computer evaluation to yield the crack size, l, σ and E, as a function of the time of loading. The values of stress, $\sigma(t)$, was calculated on the basis of the criterion

$$K_I = K_{IC} \quad (12)$$

where K_{IC} is the critical stress-intensity factor, with the fracture stress, σ_f, defined as

$$\sigma_f = K_{IC} Y^{-1} l_f^{-1/2} \quad (13)$$

where l_f refers to the crack size at fracture.

The analytical results presented above are illustrated by means of a numerical example for a polycrystalline aluminium oxide at 1400° C with property data and other parameter values as listed in Table I, obtained from various literature sources [27, 37, 38]. The values of K_{IC} and N at 1400° C were obtained by a linear extrapolation of literature data. Because the scanning electron micrographs show the cracks to be

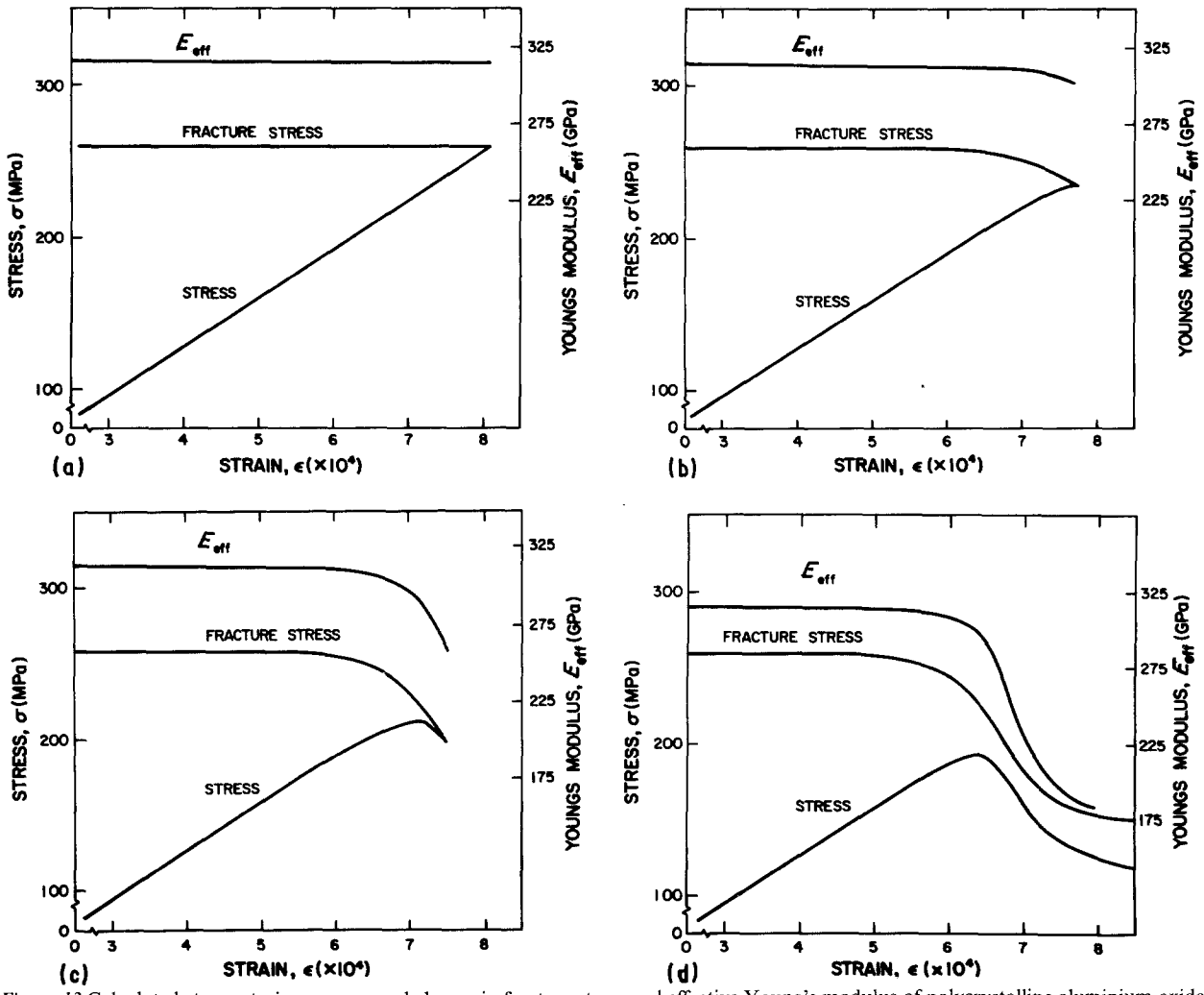

Figure 13 Calculated stress–strain response and change in fracture stress and effective Young's modulus of polycrystalline aluminium oxide simultaneously undergoing Coble creep and multiple sub-critical crack growth for a range of strain rates $\dot{\varepsilon}$ = (a) 3, (b) 3×10^{-2}, (c) 9×10^{-3}, (d) 3×10^{-3} min^{-1}.

much larger than the grain size, the value of the initial crack radius was arbitrarily chosen as equal to 50 μm.

Figs 13a, b, c and d, for the arbitrarily selected initial value of $\alpha_0 = 0.05$, show the stress–strain curves for values of the strain rate equal to 3, 3×10^{-2}, 9×10^{-3} and 3×10^{-3} min^{-1}, respectively, calculated with the aid of Equations 8 and 11. Included in the figures is the decrease in fracture stress with increasing strain, resulting from the amount of crack growth calculated from Equation 13. Fracture at $K_I = K_{IC}$ occurs at the value of strain which corresponds to the intersection of the two curves. At the highest value of strain rate the time to failure is sufficiently short so that no significant crack growth has occurred. As a result, the stress–strain curve in Fig. 13a is linear and the fracture stress is invariant with increasing strain. At the somewhat lower strain-rate of 3×10^{-2}, the stress–strain curve exhibits a slight degree of non-linearity, accompanied by a small decrease in fracture stress with increasing strain. At the even lower strain of 9×10^{-3} min^{-1}, as shown in Fig. 13c, just prior to failure the stress exhibits a decrease with increasing strain. At the lowest value of strain rate, this decrease in stress with increasing strain is such that the stress–strain curve never intersects the curve for the strain dependence of the fracture stress. Therefore, for this value of strain rate the condition of failure at $K_I = K_{IC}$ is never reached. The cracks will propagate sub-critically only, with specimen separation occurring when the cracks have traversed a distance equal to the dimension of the specimen.

Fig. 14 is a log–log plot of the fracture stress as a function of strain rate, for values of α_0 ranging from 0 to 0.1. At the highest values of strain-rate of > 0.3 min^{-1}, the fracture stress is almost independent of the strain rate and the value of α_0, because the time-to-failure is too short to permit significant crack growth. Over the range of lower values of strain rate, the fracture stress is reduced significantly, the relative decrease increasing with increasing value of α_0. Also indicated in Fig. 14 is the minimum value of strain rate at which failure still occurs at $K_I = K_{IC}$. Below this value of strain rate the cracks will propagate sub-critically only, as discussed earlier in the context of the stress–strain and fracture stress–strain curves shown in Fig. 13d.

As discussed earlier, the slope of the log fracture stress–log strain rate curve yields the value for the critical stress-intensity factor exponent, N. However, the curves in Fig. 14 indicate that at any given value of strain rate the value of the slope depends strongly on the value of α_0. The magnitude of the slope increases strongly with increasing value of α_0, i.e., with the degree to which the magnitude of the failure stress is affected by multiple crack growth.

Using Equation 3, an equation that ignores the effect of multiple crack growth, to calculate N for $\alpha_0 = 0$ and the strain rates given in Fig. 14, a value of $N = 10$ (the value used to generate the curves) is calculated only for the lowest value of strain rate. However, at the lowest values of strain rate for which failure still occurs at $K_I = K_{IC}$ and higher values of α_0, i.e. $\alpha_0 = 0.02$, 0.05 and 0.1, Equation 3 predicts N values of 6.1, 2.7 and 1.5, respectively, all far less than the actual value of $N = 10$. The results indicate that the value of N can be grossly underestimated if the effect of crack formation is ignored when calculating N.

Although direct quantitative comparisons between the experimental data and the analytical model should be approached with caution, both indicate that multiple crack formation and associated strain softening can contribute significantly to the strain-rate sensitivity of the failure stress.

In general, it is expected that the relative contributions of creep and crack growth will vary from material to material. For purposes of a quantitative comparison between experimental and calculated values of N an analysis for deformation in bending is required, which requires detailed information on the spatial variation of Young's modulus and the shift in position in the neutral axis as crack growth proceeds. Also, due to the usual assumption that plane sections remain plane, the deformation by creep and crack formation in the cracked tensile zone is expected to be coupled with the diffusional creep within the regions of the specimen subjected to compressive stress. Such an analysis is outside the scope of the present investigation.

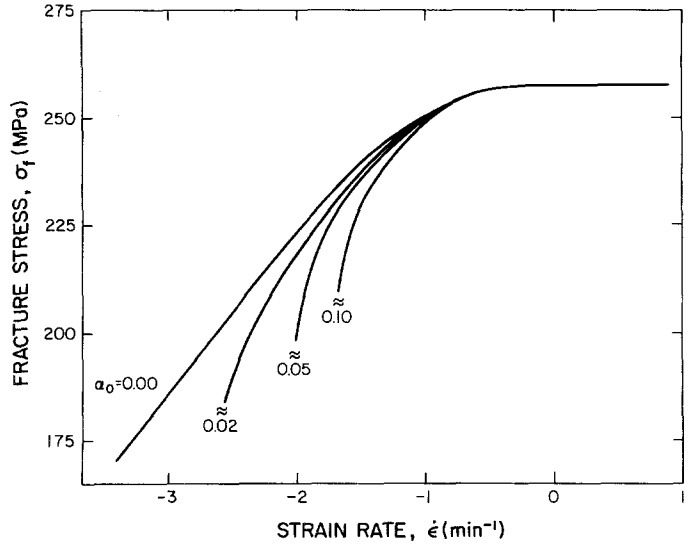

Figure 14 Log–log plot of calculated strain-rate dependence of polycrystalline aluminium oxide undergoing simultaneous deformation by Coble creep and multiple sub-critical crack growth for a range of initial values of α_0 in $E_{eff} = E_0 (1 + \alpha_0)^{-1}$. $K_I < K_{IC}$ at lower strain rates.

The results of this study suggest that in studies of the deformation and fracture of polycrystalline structural ceramics at elevated temperature, it is essential that the extent of multiple crack formation be established for proper quantitative interpretation of the experimental data. Such crack formation not only is expected to affect the strain-rate sensitivity, as suggested by the results of this study, but also the creep characteristics under constant load [39–41].

Acknowledgement

This study was supported by the Army Research Office under Contract DAAG 29-85-K-0106.

References

1. R. C. BRADT, A. G. EVANS, D. P. H. HASSELMAN, F. F. LANGE (eds), Fracture Mechanics of Ceramics", Vols. 1–8 (Plenum, New York, 1974, 1978, 1983, 1986).
2. J. E. RITTER Jr and M. S. CAVANAUGH, *J. Amer. Ceram. Soc.* **59** (1976) 57.
3. J. T. A. POLLOCK and G. F. HURLEY, *J. Mater. Sci.* **8** (1973) 1595.
4. J. E. RITTER Jr and J. N. HUMENIK, *ibid.* **14** (1979) 626.
5. J. E. RITTER Jr, G. S. GLAESEMANN, K. JAKUS and P. RAMPONE, *Phys. Chem. Glasses* **27** (1986) 65.
6. J. E. RITTER Jr, in "Fracture Mechanics of Ceramics", Vol. 4, edited by R. C. Bradt, D. P. H. Hasselman, F. F. Lange (Plenum, New York, 1978) pp. 667–86.
7. A. G. EVANS, *Int. J. Fracture* **10** (1974) 251.
8. G. SIH, "Methods of Analysis and Solutions for Crack Problems, Mechanics of Fracture, I" (Noordhoff, Leiden, 1973).
9. H. L. EWALDS and R. J. H. WANHILL, "Fracture Mechanics" (Edward Arnold London, Baltimore, 1983).
10. K. HELLAN, "Introduction to Fracture Mechanics" (McGraw-Hill, New York, 1984).
11. A. G. EVANS, in "Fracture Mechanics of Ceramics", Vol. 3, edited by R. C. Bradt, D. P. H. Hasselman, F. F. Lange (Plenum, New York, 1978) pp. 303–31.
12. *Idem*, in "Proceedings of the Sixth Army Materials Technology Conference; Ceramics for High-Performance Applications III: Reliability", edited by E. M. Lenoe, R. N. Katz and J. J. Burke (Plenum, New York, 1983) pp. 475–502.
13. *Idem, Acta Metall.* **26** (1978) 1845.
14. F. F. LANGE, in "Fracture Mechanics of Ceramics", Vol. 2, edited by R. C. Bradt, D. P. H. Hasselman and F. F. Lange (Plenum, New York, 1974) pp. 599–612.
15. Z. P. BAZANT, *J. Eng. Mech. Div. ASCE* **102** (1976) 331.
16. Z. P. BAZANT and B. H. OH, *ibid.* **110** (1984) 1015.
17. A. G. EVANS, *Acta Metall.* **28** (1980) 1155.
18. T. J. CHUANG, K. I. KAGAWA, J. R. RICE and L. B. SILLS, *ibid.* **27** (1979) 265.
19. J. B. WALSH, *J. Geophys. Res.* **70** (1965) 381.
20. R. L. SALGANIK, *Izv. Akad. Nauk. SSR, Mekh. Tverd, Tela.* **8** (1973) 149.
21. B. BUDIANSKY and R. J. O'CONNELL, *Int. J. Solid. Struct.* **12** (1976) 81.
22. D. P. H. HASSELMAN and J. P. SINGH, *Amer. Ceram. Soc. Bull.* **58** (1979) 856.
23. J. A. KUSZYK and R. C. BRADT, *J. Amer. Ceram. Soc.* **56** (1973) 420.
24. E. P. CHEN and L. M. TAYLOR, in "Fracture Mechanics of Ceramics", Vol. 7, edited by R. C. Bradt, A. G. Evans, D. P. H. Hasselman and F. F. Lange (Plenum, New York, 1986) pp. 175–86.
25. R. M. L. FOOTE, Y.-W. MAI and B. COTTERELL, *J. Mech. Phys. Solids* **34** (1986) 593.
26. K. Y. DONALDSON, A. VENKATESWARAN and D. P. H. HASSELMAN, in "Advances in Ceramics", Vol. 22, edited by V. D. Frechette and J. R. Varner (American Ceramic Society, Westerville, OH, 1988) pp. 159–75.
27. K. JAKUS, T. SERVICE and J. E. RITTER Jr, *J. Amer. Ceram. Soc.* **63** (1980) 4.
28. R. F. PABST and G. POPP, in "Fracture Mechanics of Ceramics", Vol. 5, edited by R. C. Bradt, A. G. Evans, D. P. H. Hasselman and F. F. Lange (Plenum, New York, 1983) pp. 305–15.
29. A. G. EVANS and S. M. WIEDERHORN, *J. Mater. Sci.* **9** (1974) 1270.
30. G. GRATHWOHL, in "Deformation of Ceramic Materials III", edited by R. E. Tressler and R. C. Bradt (Plenum, New York, 1984) pp. 573–86.
31. R. C. FOLWEILER, *J. Appl. Phys.* **32** (1961) 773.
32. W. D. KINGERY, H. K. BOWEN and D. R. UHLMANN, in "Introduction to Ceramics" (Wiley, New York, 1976) p. 808.
33. R. L. COBLE, *J. Appl. Phys.* **34** (1964) 1679.
34. T. G. LANGDON and F. A. MOHAMED, *J. Mater. Sci.* **13** (1978) 473.
35. R. A. SACK, *Proc. Phys. Soc. London* **58A** (1946) 729.
36. W. G. GROEBNER and N. HOFREITER, "Tables of Integrals", Part I (Springer, New York, 1975).
37. A. G. EVANS, M. LINZER and L. R. RUSSELL, *Mater. Sci. Engng* **15** (1974) 253.
38. T. G. LANGDON, *Metals Forum* **2** (1978) 59.
39. J. WEERTMAN, *Trans. Amer. Soc. Mater.* **62** (1969) 502.
40. A. VENKATESWARAN and D. P. H. HASSELMAN, *J. Mater. Sci.* **16** (1981) 1627.
41. D. P. H. HASSELMAN, *ibid.* **18** (1983) 161.

Received 21 December 1987
and accepted 6 May 1988